BABEŞ-BOLYAI UNIVERSITY

FACULTY OF ENVIRONMENTAL SCIENCE AND ENGINEERING

DOCTORAL SCHOOL OF ENVIRONMENTAL SCIENCE

DOCTORAL THESIS SUMMARY

Methods and techniques of identifying and analysing oil smoke plumes using synergic satellite data

PhD COORDINATOR

Prof. univ. dr. ing. Ozunu Alexandru

PhD CANDIDATE

Mereuță Alexandru

Cluj-Napoca

2023

TABLE OF CONTENTS OF THE DOCTORAL THESIS

Key words

Hazard and Risk

Earth Observing Satellites

Atmospheric Aerosols

Oil Smoke Plumes

Smoke aerosol Typing

PM2.5 Concentrations

Air Quality

1. Intoduction

Emissions of potentially hazardous substances, both in gaseous and condensed form, contribute to the increase in concentrations of minor gases and particles. These anthropogenic concentrations are the primary source of impact on global climate change and air quality degradation.

Defining the types of aerosols is a challenging task due to their high degree of variability in composition and concentration, resulting from different atmospheric residence times, dry and wet deposition, diverse sources and emission rates, transport trajectories, and seasonal variability (Dutkiewicz et al., 2009; Li et al., 2015; Mereuţă et al., 2022; Samset et al., 2018).

The health effects associated with both short-term and long-term exposure to aerosols have been extensively documented in scientific literature (Brauer et al., 2016; Zhang and Batterman, 2013).

However, the scientific understanding of the impact of aerosols on global climate change is notably limited, with significant uncertainties. The humanitarian community, as well as disaster response efforts, are increasingly relying on Earth Observation (EO) satellite systems to assess the impact and to plan and coordinate emergency response activities following major natural and anthropogenic disasters worldwide.

In this context, the doctoral thesis presents a novel methodology for identifying and analysing smoke from oil fires using synergistic satellite data. The thesis proposes this approach by considering the advantages of global coverage offered by these techniques and the application of existing retrieval algorithms. Thus, quantifying the properties of the studied aerosols, defining their typology, and estimating the concentrations of particulate matter improve the current knowledge in the field, while also laying the foundation for a new application for delineating and quantifying the hazards associated with these events.

1.1 Objectives

One of the main objectives of this study is to highlight the importance of satellite remote sensing techniques in identifying these types of events. Petrochemical installations can be located in desert areas, at sea, or in hard-to-reach locations, far from air quality monitoring stations or AErosol RObotic NETwork (AERONET) stations (Holben et al., 1998). In-situ approaches, ground stations, and modelling tools are largely inaccessible in conflict-prone or high-risk health areas. In addition to this advantage, a synergistic approach using different types of satellite instruments can provide three-dimensional spatial coverage (Mereuţă et al., 2022). This study will focus on the use of MODIS and CALIPSO products regarding these types of aerosols, also emphasizing methodological limitations. Using data from both the MODIS instruments aboard the Terra and Aqua satellites, we addressed the temporal evolution of smoke plumes. Through CALIPSO data, we evaluated the specific lidar properties and altitude development of smoke plumes (Mereuţă et al., 2022). At the current level of science, we have not identified any other similar studies specifically focusing on the retrieval of aerosol properties resulting from major petrochemical accidents using a synergistic approach with satellite products (Mereuţă et al., 2022). Determining the optical and microphysical properties of these smoke plumes is important for improving models estimating the atmospheric radiative budget. These models are particularly important for global climatological studies and associated potential effects. Additionally, accurate quantification of this type of aerosol can lead to improved satellite retrieval methods. The associated risk to human health leads to shaping another ultimate objective of the doctoral thesis. Thus, the study proposes a method for estimating the concentrations of particulate matter and delineating the zones influenced by the hazard. For the air quality research community, this study can provide a new technique for observing black carbon and can be used synergistically to describe the temporal and spatial evolution of such pollutant plumes (Mereuţă et al., 2022).

2. Theory

Earth Observation (EO) satellites provide a privileged viewpoint for monitoring multiple geophysical variables, including in hard-to-access areas of the globe. EO data provides information about the state of the environment and its changes, thus contributing to the design and development of environmental policies or the environmental dimension of other policies (Tassa, 2020). For example, they can inform efforts dedicated to the conservation of natural resources (Finer et al., 2018), support emergency management and the planning of disaster risk reduction measures (Muthike, 2015).

Atmospheric aerosols are complex mixtures of solid and liquid particles suspended dynamically in the air. They originate from both natural and anthropogenic emissions (Mereuţă et al., 2022). The most common forms of aerosols are fog, dust, sea salt, biological exudates, and smoke (biomass burning). Smog and black carbon are usually the result of industrial and transportation activities (Wei et al., 2020). Distinct species such as black carbon (BC), organic carbon (OC), sulfates, nitrates, trace elements, sea salt, mineral dust, and biological matter undergo atmospheric modifications, resulting in different combinations of compounds (Mereuţă et al., 2022). Aerosols have a direct effect on radiation distribution through scattering, absorption, and emission of light within the atmosphere (Mereuţă et al., 2022). Additionally, they can impact the climate system through indirect effects such as the formation of cloud condensation nuclei, influence on cloud lifetime and properties, disturbance of atmospheric stability, and precipitation factors (Samset et al., 2018).

Global particle emissions have been dominated by the burning of fossil fuels (primarily coal) and biomass burning. It is estimated that these emissions will double by 2040, largely due to anticipated increases in fossil fuel burning, expected mainly in China and India (Ramanathan and Carmichael, 2008).

Smoke from oil substances and biomass burning (BB) significantly differ in the OC/BC ratio. Studies have shown values ranging from 3 to 20 for BB (Andreae, 2019; Konovalov et al., 2018), depending largely on the types of fuel. As for smoke from oil

products, the OC/BC ratios are much lower, ranging from 0.83 to 1.05 (Daum et al., 1993; Ferek et al., 1992; Laursen et al., 1992), also depending on the types of fuel (Mereuţă et al., 2022). Studies also report a high BC content in these smoke plumes, where BC represents 46-50% of the total PM content for Kuwait oil fires (Hobbs and Radke, 1992; Laursen et al., 1992; Stevens et al., 1993), up to 50-75% for the Bouncefield fire (Mather et al., 2007), and 75-82% for plumes generated by surface oil burning over the ocean (Gullett et al., 2017, 2016; Ross et al., 1996).

Due to their complex influences on the environment and climate system, assessing key aerosol parameters is essential for any atmospheric study. Aerosol Optical Depth (AOD), the vertically integrated extinction over the entire atmospheric column, is a strongly correlated parameter with PM concentrations (Mereuţă et al., 2022). Together with other properties such as the Angstrom Exponent (AE), single scattering albedo (SSA), size distribution, and vertical concentration variations, we can better describe their atmospheric impact. Since the 1970s, there have been a significant number of satellite sensors successfully used for retrieving AOD and other aerosol properties (Wei et al., 2020). To choose among various specific aerosol products, one must consider the variety of sensors and their characteristics, such as spatial, temporal, and spectral resolutions, scanning methods (single or multi-view), intensity or polarimetric design, and different retrieval algorithms (Sogacheva et al., 2020; Wei et al., 2020).

3. Event description

This section will summarize a collection of events between 2008 and 2020 that have been successfully identified using satellite remote sensing techniques. Following these events, a range of optical and microphysical properties of the resulting smoke plume were retrieved, and statistical analyses were performed to better describe these types of aerosols (Mereuţă et al., 2022). The characteristics of the events are summarized in Table 1.

Nr. ID	Location	MODIS observations		Coordinates	Cause	Installation type
		Start	End			
1	Qayyara, Iraq	13.06.2016	27.03.2017	35.83 N ; 43.21 E	Armed conflict	Oil wells
2	Omidieh, Iran	06.05.2019	06.05.2019	30.84 N ; 49.65 E	Human error	Pipeline
3	Haradh, Hawiyah, Uthmaniyah, Shedgum, Buqayq; Arabia Saudită	14.09.2019	26.09.2019	24.05 N ; 49.20 E 24.80 N ; 49.35 E 25.18 N ; 49.31 E 25.64 N ; 49.39 E 25.92 N ; 49.68 E	Armed conflict	Oil refinery
4	Caspian Sea, Azerbaijan	06.12.2015	18.12.2015	40.20 N ; 51.06 E	Storm	Ocean rig
5	Gulf of Mexico, USA	21.04.2010	21.04.2010	28.44 N ; 88.21 W	Equipment failure	Ocean rig
6	Marea Chinei de Est, China	14.01.2018	14.01.2018	28.37 N ; 126.08 E	Human error	Oil Tanker
7	Houston Texas, USA	18.03.2019	19.03.2019	29.43 N ; 95.05 E	Equipment failure	Oil tank
8	Jaipur, India	30.10.2009	08.11.2009	26.77 N ; 75.83 E	Human error	Oil tank
9	Sendai, Japan	12.03.2011	13.03.2011	38.27 N ; 141.03 E	Earthquake, tsunami	Oil tank
10	Vasylkiv, Ukraine	09.06.2015	10.06.2015	50.16 N ; 30.32 E	Sabotage	Oil tank
11	Ra's Lanuf, Libya	19.08.2008	25.08.2008	30.45 N ; 18.49 E	Human error	Oil tank
12	Ra's Lanuf, Libya	12.03.2011	14.03.2011	30.45 N ; 18.49 E	Armed conflict	Oil tank
13	As Sidr, Libya	26.12.2014	31.12.2014	30.60 N ; 18.28 E	Armed conflict	Oil tank
14	Ra's Lanuf, As Sidr; Libya	05.01.2016	07.01.2016	30.45 N ; 18.49 E 30.60 N ; 18.28 E	Armed conflict	Oil tank
15	Surt disrtric, Libya	14.01.2016	14.01.2016	30.02 N ; 18.50 E	Armed conflict	Pipeline
16	Ra's Lanuf, Libya	21.01.2016	23.01.2016	30.45 N ; 18.49 E	Armed conflict	Oil tank
17	Ajdaviya district, Libya	01.02.2016	01.02.2016	29.68 N ; 20.54 E	Armed conflict	Pipeline
18	Ra's Lanuf, Libya	17.06.2018	21.06.2018	30.45 N ; 18.49 E	Armed conflict	Oil tank
19	Puebla, Mexico	19.12.2010	19.12.2010	18.96 N ; 98.45 W	Crime	Pipeline
20	Escravos, Nigeria	04.01.2018	05.01.2018	5.45 N ; 5.35 E	Forest fire	Pipeline
21	Puerto Sandino, Nicaragua	18.08.2016	19.08.2016	12.18 N ; 86.75 W	Unknown	Oil tank
22	Golful Oman	13.06.2019	13.06.2019	25.39 N ; 57.38 E	Armed conflict	Oil Tanker
23	Catano, Puerto Rico	23.10.2009	24.10.2009	18.41 N ; 66.13 W	Human error	Oil tank
24	Punto Fijo,Venezuela	27.08.2012	27.08.2012	11.74 N ; 70.18 W	Equipment failure	Oil tank
25	Butcher Island, India	07.10.2017	08.10.2017	18.95 N ; 72.90 E	Lightning strike	Oil tank

Table 1. Major industrial events leading to observable smoke plumes seen in MODIS RGB images.

4. Methods and techniques used in this study

4.5 The synergic method developed

Figure 1 presents a synopsis of each stage of the analysis, starting from a collection of events identified in scientific literature as well as in local media articles. We selected a time interval of 12 years during which both MODIS and CALIPSO retrieved a substantial amount of atmospheric data from the smoke plumes (Mereuţă et al., 2022). Using MODIS RGB images, we can visually identify each event (Table 1) (Mereuţă et al., 2022). The two MODIS sensors aboard the Aqua and Terra platforms were used because they possess several advantageous features for event identification and analysis: global daily coverage, good pixel resolution, algorithmic maturity, two retrieval windows, and a large data archive (20 years of mission). CALIPSO data were utilized to compare the AOD of the plumes and to fill in gaps in the MODIS data, such as smoke thickness and elevation, scene classification, and aerosol type classification (using lidar ratio and particle depolarization ratio). The events identified in the literature were selected based on the size analysis of the plume and specific retrieval conditions. We selected plumes with a coverage area larger than 500 km^2 for statistical relevance, as smaller plumes resulted in a limited number of pixels in the retrieved data. Events were excluded if the atmospheric scene was predominantly cloudy, with a coverage exceeding 50% (Mereuţă et al., 2022). We considered "successful retrievals" as those data retrievals that produced non-zero values of AOD pixels, with a certain degree of variation (for at least 50% of the smoke plume pixels, AOD values should vary, resulting in value differences of at least 0.01), overlapping with the plume area. We considered an "unsuccessful retrieval" if the retrieval over the plume area did not yield AOD data (after cloud screening) or if the AOD values were less than 0.1 and the resulting pixels exhibited a high degree of homogeneity (e.g., over 90% of the plume pixels had a fixed AOD value of 0.09). We used both successful and unsuccessful retrievals to highlight the capabilities and limitations of the MODIS sensors (Mereuţă et al., 2022).

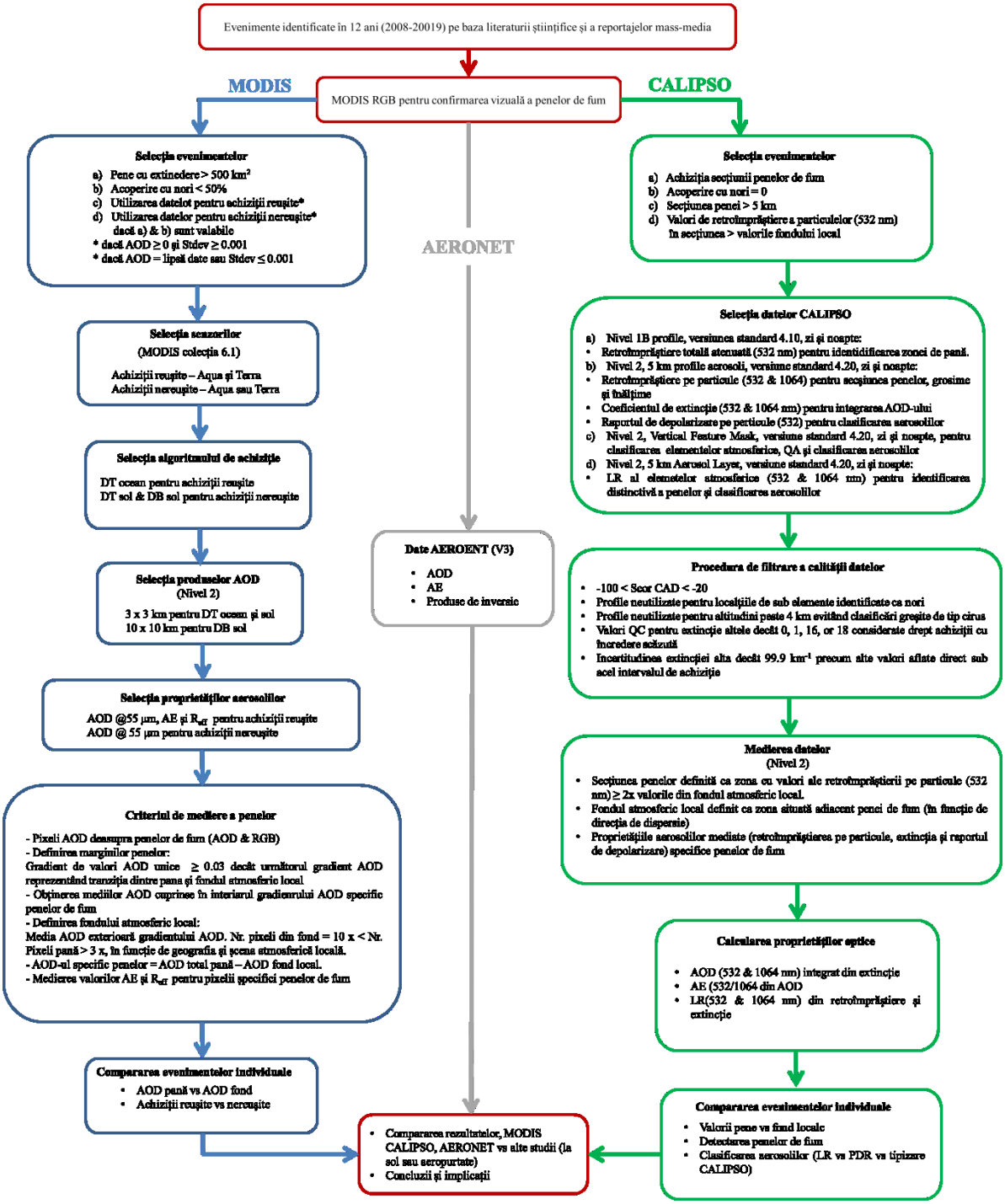

Figure 1. Flowchart of the plume analysis method

5. Results and discussions

5.1 Descriptive case study

Based on the information presented in Table 1, we filtered a total of 375 days in which oil smoke plumes were observed by the MODIS sensors. After applying the selection criteria for the MODIS sensor, we obtained a total of 10 days with successful retrievals. The majority of oil smoke plumes resulted in unsuccessful retrievals, 70.7%, while 26.7% of them were eliminated due to a high percentage of cloud coverage (Mereuţă et al., 2022). By applying the selection criteria for CALIPSO, we obtained a number of 6 sections of suitable smoke plumes for analysis (Mereuţă et al., 2022). Table 2 presents the retrieval dates of MODIS and CALIPSO suitable for analysis.

Table 2. List of successful MODIS retrievals and CALIPSO overpass dates.

Nr. event	MODIS (Terra & Aqua) Retrieval date	CALIPSO retrieval date
		01.07.2016
1	-	17.07.2016
		21.10.2016
4	08.12.2015	-
5	21.04.2010	-
9	11.03.2011	-
11	-	22.08.2008
	28.12.2014	-
13	29.12.2014	29.12.2014
	30.12.2014	-
14	06.01.2016	06.01.2016
16	21.01.2016	-
20	19.08.2016	-
21	04.01.2018 (Aqua)	-

We selected a successful retrieval to better describe the method used in our analysis. Figure 2 presents event 14, the case of the Ra's Lanuf and As Sidr tank farm fires that started on January 5, 2016, and burned throughout days 6 and 7. The image retrieval was performed on January 6 at 12:05 UTC by MODIS Aqua. Figure 2a represents a true-color composite image showing the smoke plume emanating from both locations with a dispersal direction

towards the E-NE over the Gulf of Sidra. By evaluating only this image, we can only distinguish parts of the plume that appear to be less dispersed and thus exhibit a smaller proportion of mixing with local background aerosols. In this study, we focused our attention on plume areas where high aerosol concentrations are present, while retrievals made at the edges of the plume, where background aerosols can have a significant influence on the retrieved values, were eliminated (Mereuţă et al., 2022). Therefore, Figure 2b was constructed based on the AOD (0.55 μm) retrieval and a plume edge selection technique. To determine the plume edge, we constructed isolines of AOD values from the retrieval pixels. The 3 × 3 km product is more suitable for determining AOD gradients and, therefore, was selected over the standard 10 × 10 km product. Figure 2b shows higher AOD values in the selected smoke plume area compared to the area with local atmospheric background (Mereuţă et al., 2022). At the time of retrieval, we can observe two distinct smoke plumes, a thin plume originating from As Sidr and the main plume (inside the black contour, Fig. 2b) originating from Ra's Lanuf. Since the plume from As Sidr did not meet the selection criteria, the analysis is performed for the main plume from Ra's Lanuf (Mereuţă et al., 2022). To further discriminate between the AOD values of the plume and the local background, we calculated the average of all non-plume pixel values over the water region in the Gulf area (Mereuţă et al., 2022). Then, the average AOD values were subtracted from each pixel of the AOD values over the plume region to determine the total contribution of the smoke plume. Therefore, Figure 2c illustrates the specific AOD gradient of the plume. Figures 2d and 2e show the AE (0.55/0.86 μm) and Reff (μm) that were selected for aerosol classification. For AE and Reff, we used the same edge selection technique as described above, without subtracting the local background (Mereuţă et al., 2022). AE presents very low values, indicating a dominant coarse mode, which is also highlighted by the large Reff chosen from the LUT. It is also evident from both figures that both plumes extend beyond the edge selection (Mereuţă et al., 2022). In this case, the specific plume AOD average was 0.13, while the background values averaged 0.08. Figure 2c shows AOD values of the plume up to 0.24 above the local background average for the Ra's Lanuf event. The AOD gradient in Figure 2c exhibits the

highest values at the center of the plume, where aerosol mixing is expected to be lower (Mereuţă et al., 2022). The plume's average AE was -0.18, contrasting with the local background value of 0.45, and the plume's Reff showed 1.45 µm compared to 0.51 µm for the local background.

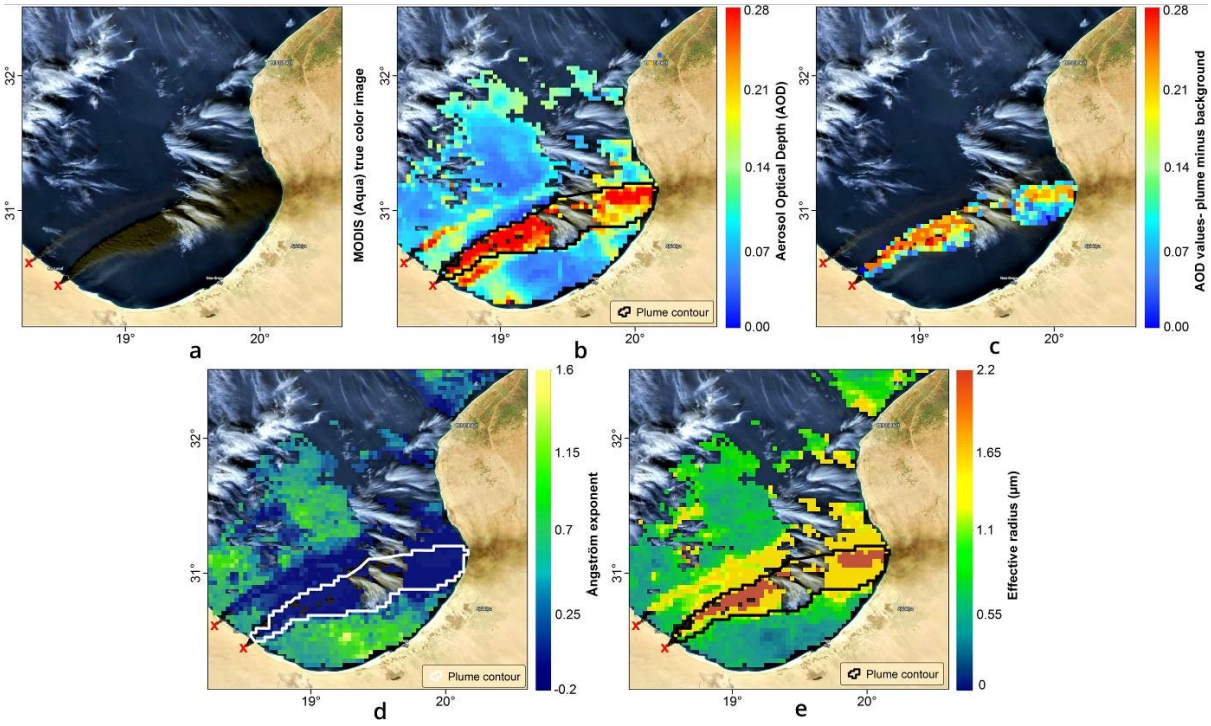

Figure 2. Visual representation of the analysis method for MODIS data: (a) plume captured in true colour; (b) AOD retrieval over the plume area and background (Gulf of Sidra); (c) AOD retrieval as a result of plume minus background values; (d) Ångström exponent for plume and background area; (e) effective radius for plume and background area. The red coloured "x" indicates the event origin (satellite imagery from the NASA Worldview application, https://worldview.earthdata.nasa.gov, last access: 5 January 2022).

Figure 3 presents an example of an unsuccessful retrieval of the algorithm for dry surfaces specific to the plume of event 13 on December 30, 2014. We can distinguish the plume from the RGB image above the Gulf of Sidra and also observe the AOD values above the land where the smoke moved E-NE towards the island of Crete. However, there doesn't seem to be a distinguishable AOD gradient above the land in the plume section (Mereuţă et al., 2022). Further inspection suggested that all pixels produced values of 0.095, indicating that the lower radiance values did not fit well with the pre-existing LUT values (Mereuţă et

al., 2022). Therefore, the region is classified as "clean atmosphere," and thus a single AOD value is assigned to all pixels. In contrast to the algorithm for land, the algorithm for ocean retrieved AOD values ranging from 0.1 to 0.37. Since these smoke plumes result from extreme scenarios, they are rarely observed, and specific conditions for radiative transfer calculations may not be reflected in the algorithm used. Therefore, we believe that there are no cases in the LUT values that describe extremely low atmospheric transmittance and radiance, strong absorbing aerosol, low SSA, and low reflectance values over a wide spectral range, including the MODIS bands 1 to 7.

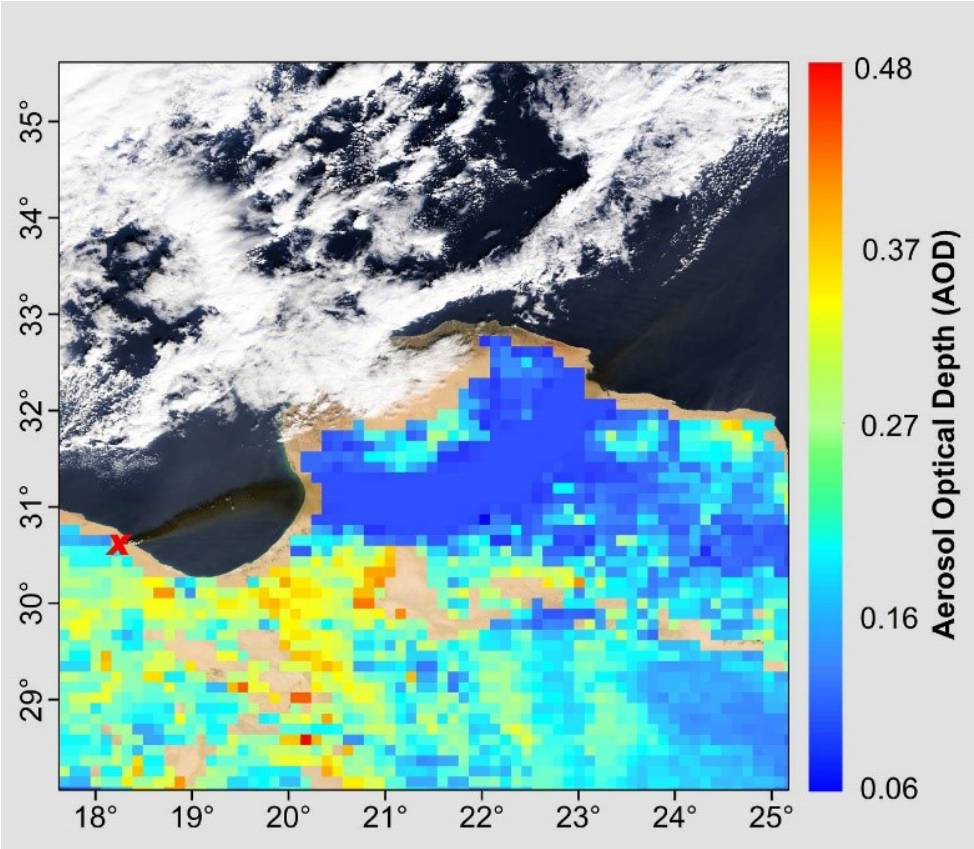

Figure 3. Retrieval of plume (unsuccessful) and background AOD values: event 13, 30 December 2014. The red coloured “x” indicates the event origin (satellite imagery from the NASAWorldview application, https://worldview.earthdata.nasa.gov, last access: 5 January 2022).

Event 14 at Ra's Lanuf and As Sidr on January 6, 2016, was also captured by CALIPSO lidar measurements as the CALIPSO overpass coincided with a cross-section of the plume area. Figure 4a presents this nearly real-time overlap as CALIPSO follows Aqua within a 2-minute time interval. Within the 15 km cross-section of the plume, we selected a particle backscatter profile for reference, Figure 4b, and based on this parameter, we determined the elevation and thickness of the plume (Mereuţă et al., 2022). The average thickness of the plume was approximately 920 m. The base of the layer was situated between 2600 and 3100 m above the Gulf, while the upper part was measured between 3300 and 4200 m (Mereuţă et al., 2022). The entire cross-section of the plume is presented in Figure 5a. We observe the main plume from Ra's Lanuf elevated between 2600 m and 4200 m (Mereuţă et al., 2022). Figure 5a also shows the secondary plume from As Sidr, located 0.2º north of the main one, and situated around 2000 m (Mereuţă et al., 2022). Based on CALIPSO measurements of the main plume, the average values of the particle backscatter coefficient (532 nm) were 0.015 $km^{-1}sr^{-1}$, while the values at 1064 nm were 0.017 $km^{-1}sr^{-1}$. The average values of the extinction coefficient at 532 nm were measured at 1.65 km^{-1}, while the 1064 nm channel provided a value of 1.55 km^{-1} (Mereuţă et al., 2022). The presented event is an example of an opaque layer of aerosols where the lidar was unable to penetrate to the sea surface over the Gulf of Sidra (Mereuţă et al., 2022). This event recorded a lidar ratio of 109 ± 47 sr at 532 nm and 86 ± sr at 1064 nm. These values are higher than the CALIPSO V4 aerosol subtype values for: elevated smoke 70 ± 16 (532 nm) and 30 ± 18 (1064 nm); polluted/anthropogenic smoke 70 ± 25 (532 nm) and 30 ± 18 (1064 nm) (Kim et al., 2018; Mereuţă et al., 2022). The initial lidar ratios were reduced by 5% based on the scheme described by Young et al. (2018) for opaque aerosol layers. These events are described as rare (1% of all unique aerosol layers detected in 2012; Young et al., 2018) and may be subject to additional uncertainties. The initial value of the lidar ratio (SP) is described by Young et al. (2018) in Equation (1) (Mereuţă et al., 2022). This assumes a zero value for transmittance in both directions (TP2 = 0) and a multiple scattering factor value of 1 ($\eta = 1$). Young et al. (2018) also suggest that assuming $\eta = 1$ may not hold for opaque aerosol layers

and may introduce bias errors (Mereuţă et al., 2022). These errors can propagate through the retrievals of extinction and AOD and may result in more conservative estimates. The particle depolarization ratio for the plume from Ra's Lanuf was 0.11 ± 0.43, corresponding to moderately depolarized smoke (Kim et al., 2018; Mereuţă et al., 2022). Figure 5c shows the classification of CALIPSO atmospheric features, while Figure 5b presents the aerosol classification results.

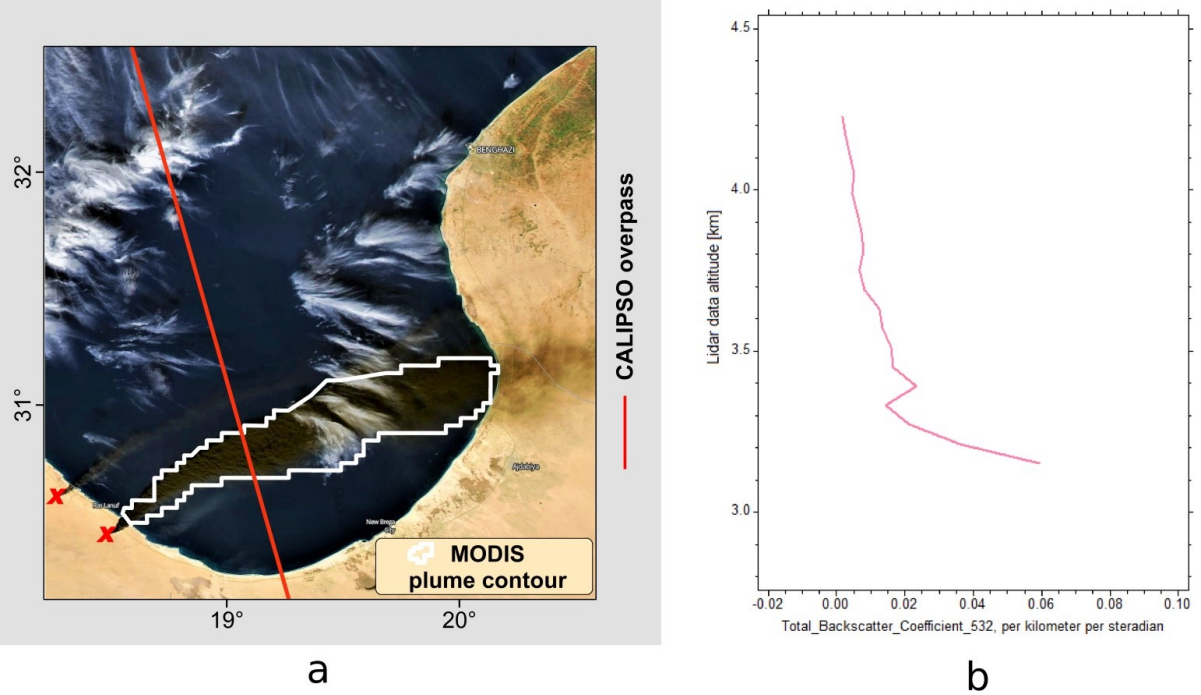

Figure 4 (a) CALIPSO overpass and MODIS plume contour, (b) Particulate backscatter coefficient profile CALIPSO level 2 (532 nm) (satellite imagery from the NASA Worldview application, https://worldview.earthdata.nasa.gov, last access: 5 January 2022).

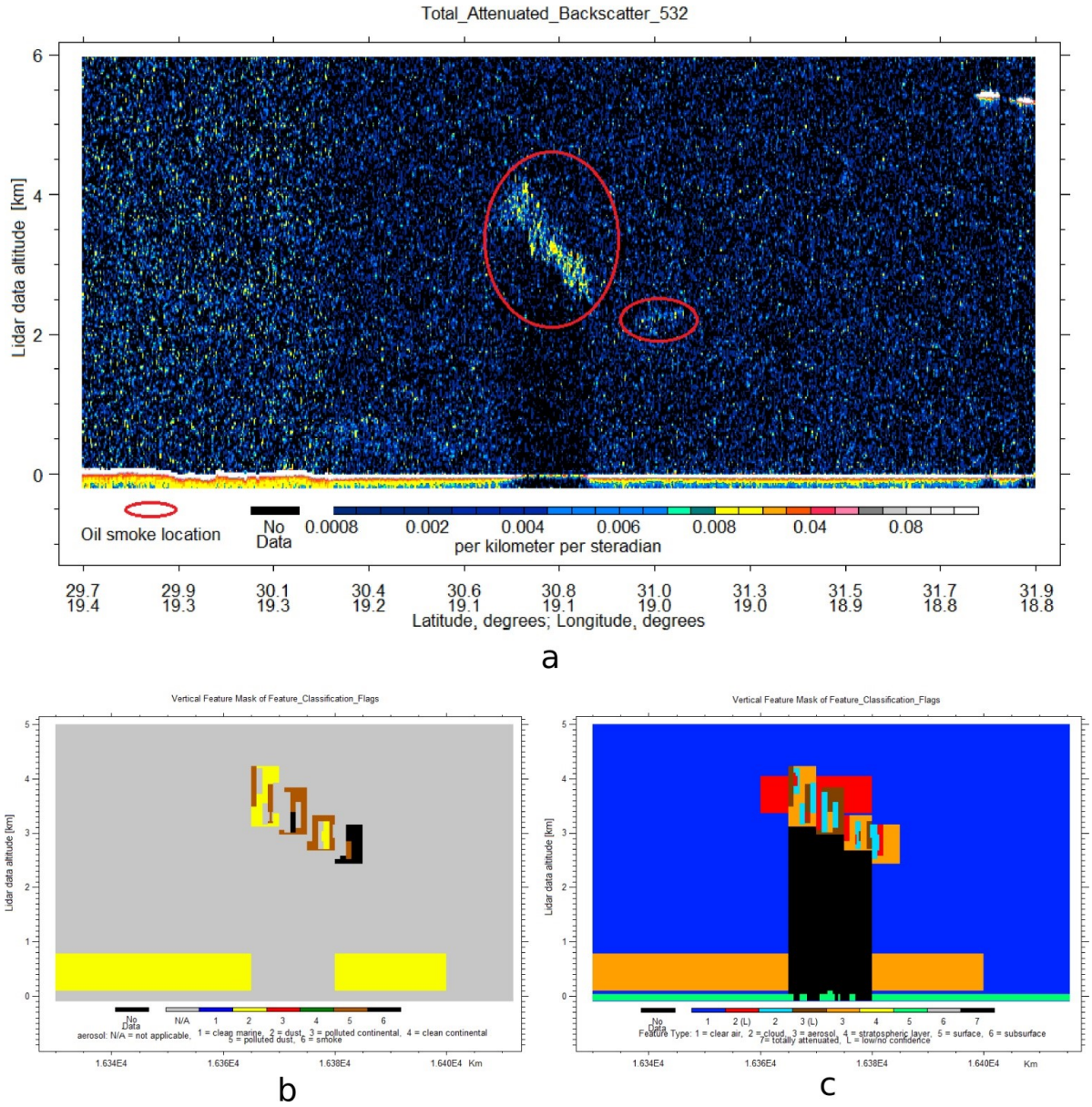

Figure 5 (a) Image of event 14 plume based on CALIPSO total attenuated backscatter (532 nm) vs. lidar data altitude data. (b) Aerosol feature classification. (c) Cloud feature classification.

Based on these images and the average CAD score of -48, the smoke plume is classified as a mixed cloud and aerosol feature. This is expected as water vapour and particulate matter are primary components of petrochemical combustion emissions (Daum et al., 1993; Ferek et al., 1992; Mereuţă et al., 2022). Cloud formations above the oil smoke, such as pyroCb (pyrocumulonimbus), have been observed in other cases, as shown in Figure 6, a phenomenon that hinders the retrieval of AOD in both passive and active sensors.

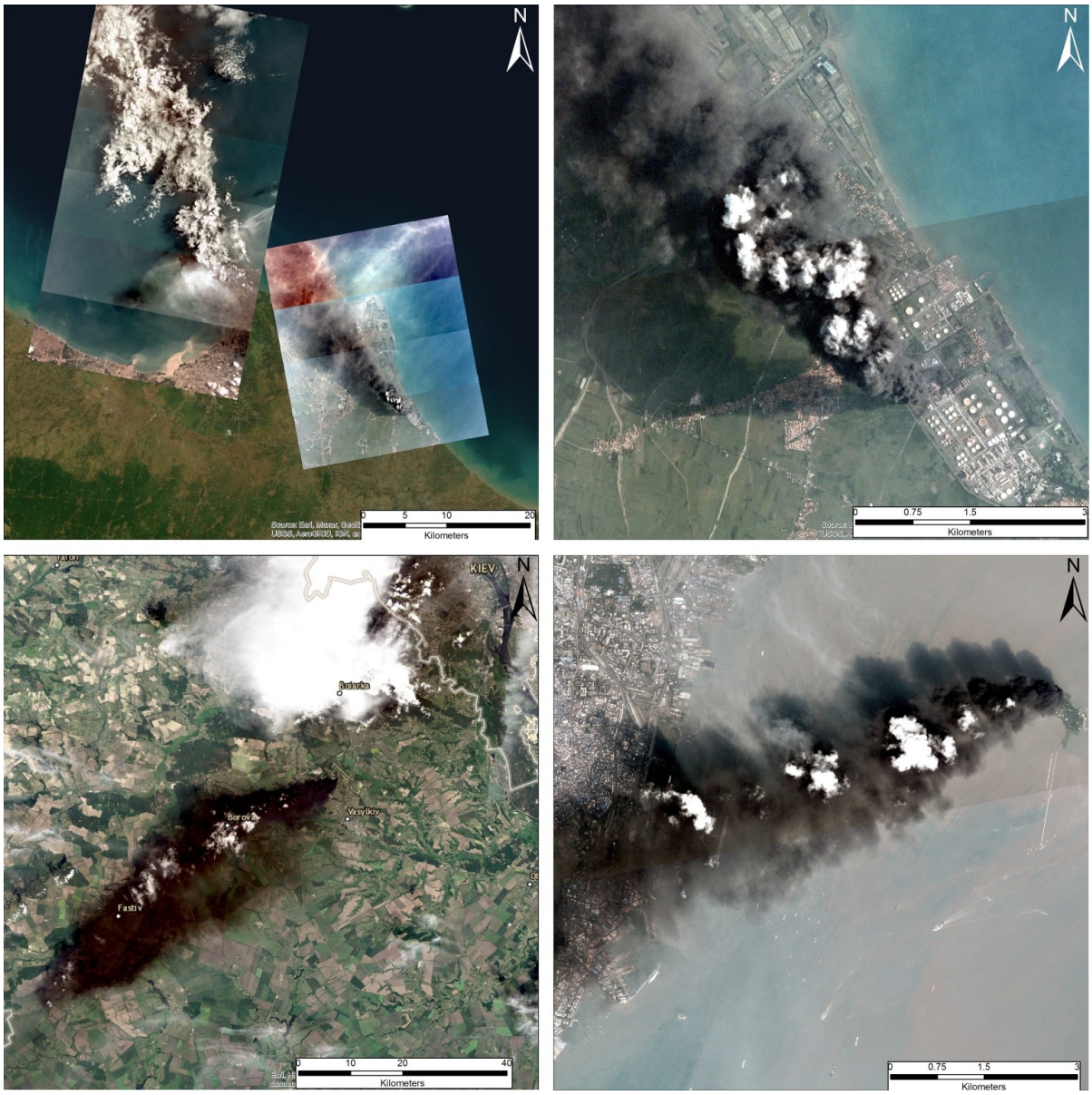

Figure 6. Cloud formation on top of oil smoke plumes. Upper images depicting the fire at Balongan, Indonesia, 29 March 2021; lower left image depicting the fire at Vasylkiv, Ukraine, on 9 June, 2015; lower right image depicting the fire at Butcher Island, India, on 7 October 2017 (satellite imagery from OpenStreetMap©OpenStreetMap contributors, 2021. Distributed under the Open Data Commons Open Database License (ODbL) v1.0 and Planet Team, https://www.planet.com/, last access: 5 January 2022).

The current version of the vertical feature mask provides a mixed result for aerosol classification, including dust, polluted dust, and smoke aerosols for this plume. The average

AOD values of the plume range from 1.52 ± 0.8 (532 nm) to 1.43 ± 0.47 (1064 nm) (Mereuță et al., 2022). We also calculated the AE (532/1064) of the plume, yielding a value of 0.09, indicating the presence of coarse particles.

5.2 MODIS successful retrievals

The successful MODIS retrievals are presented in Tables 3 and 4 as mean values and standard deviations. The MODIS Aqua retrieval presented in Section 5.1 was consistent with the Terra retrieval. Event 14 showed a larger difference in specific plume AOD values between the Terra and Aqua retrievals. However, this was expected as the fire spread to multiple oil reservoirs during the two retrievals. Based on these results, we did not identify significant discrepancies between the two sensors (Mereuţă et al., 2022). For the plume area and specific plume AOD, most values fall within the expected uncertainty range of the retrieval algorithm, ± (0.05 + 0.20 × AOD), when comparing between the two sensors (Gupta et al., 2018). Small changes in AOD values can also be attributed to plume dispersion. In most cases, the specific plume AOD is the main contributor to the total AOD in the atmospheric column, although all AOD values are generally low. In cases where the background AOD is already low, a thin layer of black smoke can reduce atmospheric transmittance and radiance values. This effect would lead to lower top-of-atmosphere reflectance and specific plume AOD values (Mereuţă et al., 2022).

Table 3. Mean and standard deviation values of aerosol properties (AOD, AE, Reff) based on MODIS Terra successful retrievals

Nr. event	Date	Plume AOD	Background AOD	AOD (plume specific)	AE plume	AE bacground	R_{eff} plume (μm)	R_{eff} background
4	08.12.2015	0.19; 0.04	0.06; 0.01	0.13; 0.04	1.25; 0.18	1.59; 0.44	0.47; 0.06	0.29; 0.23
5	21.04.2010	0.25; 0.03	0.20; 0.02	0.05; 0.03	0.34; 0.25	1.17; 0.30	0.61; 0.14	0.26; 0.05
9	11.03.2011	0.29; 0.05	0.13; 0.05	0.16; 0.05	0.43; 0.30	1.64; 0.61	0.65; 0.19	0.22; 0.10
	28.12.2014	0.22; 0.05	0.07; 0.02	0.15; 0.05	-0.07; 0.15	0.68; 0.33	1.19; 0.22	0.49; 0.14
13	29.12.2014	0.13; 0.02	0.05; 0.004	0.08; 0.02	-0.03; 0.06	0.52; 0.12	1.03; 0.16	0.79; 0.10
	30.12.2014	0.18; 0.03	0.15; 0.08	0.03; 0.07	-0.11; 0.10	0.08;0.14	1.48; 0.31	0.80; 0.15
14	06.01.2016	0.12; 0.02	0.02; 0.005	0.10; 0.02	-0.18; 0.002	0.45; 0.38	1.45; 0.02	0.51; 0.16
16	21.01.2016	0.21; 0.03	0.07; 0.02	0.14; 0.03	-0.13; 0.09	1.20; 0.33	1.34; 0.29	0.36; 0.12
20	19.08.2016	0.24; 0.03	0.19; 0.04	0.05; 0.03	0.06; 0.16	0.41; 0.20	0.87; 0.12	0.61; 0.10

Table 4. Mean and standard deviation values of aerosol properties (AOD, AE, Reff) based on MODIS Aqua successful retrievals

Nr. event	Date	Plume AOD	Background AOD	AOD (plume specific)	AE plume	AE bacground	R_{eff} plume (μm)	R_{eff} background
4	08.12.2015	0.14; 0.03	0.03; 0.01	0.11; 0.03	0.96; 0.35	1.28; 0.34	0.29; 0.06	0.28; 0.14
5	21.04.2010	0.23; 0.03	0.16; 0.02	0.07; 0.03	0.74; 0.27	1.41; 0.24	0.38; 0.13	0.26; 0.06
9	11.03.2011	0.24; 0.04	0.14; 0.03	0.10; 0.04	0.50; 0.19	0.85; 0.21	0.57; 0.13	0.36; 0.09
	28.12.2014	0.11; 0.02	0.05; 0.01	0.06; 0.02	-0.13; 0.15	0.01; 0.18	1.44; 0.05	1.04; 0.16
13	29.12.2014	0.15; 0.05	0.07; 0.03	0.08; 0.05	-0.06; 0.15	0.52; 0.30	1.73; 0.45	0.70; 0.17
	30.12.2014	0.13; 0.04	0.16; 0.04	-0.03; 0.03	-0.11; 0.11	0.09; 0.14	1.37; 0.12	0.89; 0.13
14	06.01.2016	0.21; 0.05	0.08; 0.04	0.13; 0.05	-0.14; 0.08	0.38; 0.39	1.64; 0.37	0.68; 0.22
16	21.01.2016	0.15; 0.02	0.05; 0.01	0.10; 0.02	-0.15; 0.07	0.79; 0.21	1.38; 0.16	0.32; 0.07
20	19.08.2016	0.09; 0.01	0.12; 0.03	-0.03; 0.01	-0.01; 0.19	0.31; 0.34	1.17; 1.29	0.71; 0.20
21	04.01.2018	0.75; 0.09	0.79; 0.07	-0.04; 0.09	0.78; 0.29	0.67; 0.23	0.58; 0.14	0.54; 0.14

5.4 CALIPSO retrievals

Over the course of a 12-year period, we have identified three events in the Gulf of Sidra, events 11, 13, and 14. Except for event 14, described earlier in Section 5.1, all CALIPSO retrievals were unconfined (Mereuţă et al., 2022). Results specific to the smoke plumes are presented in Tables 5-7.

Based on CALIPSO measurements, the scattering and extinction coefficients of the smoke varied between 2 and 9 times higher than background levels. In four out of six cases, the particle depolarization ratio revealed values ranging from 0.11 to 0.15, indicative of moderately depolarizing smoke, while the higher values in two cases were largely determined by the presence of dust particles in the local atmospheric scene (Mereuţă et al., 2022). Except for one case, all lidar ratios were obtained through unconfined retrievals, as the plume was located within the boundary layer (Mereuţă et al., 2022). The opaque feature exhibited high lidar ratios of 109 ± 47 sr (532 nm) and 86 ± 10 sr (1064 nm), similar to the lidar ratio of smoke found in the literature (Haarig et al., 2018; Mereuţă et al., 2022). We suspect that these values are a good indicator of the strong light absorption nature specific to these aerosols. The average CAD scores ranged from -46 to -99, indicating a strong confidence in the presence of aerosols. The feature classification algorithm indicated the presence of small clouds in 3 out of the 6 cases, suggesting mixed cloud-aerosol features (Mereuţă et al., 2022). The AE values were consistently low in all cases, suggesting the presence of larger smoke particles in the cross sections of the smoke plumes. The measured AOD values ranging from 0.02 to 1.52 were directly influenced by the fuel burning rates, local aerosol loading in the background, and especially by the lidar ratio assumptions (Mereuţă et al., 2022). The smoke from event 14 was identified above the PBL up to 4200 m. This is a good indicator of the magnitude of the event, as it involved multiple fires from significant burning rates that simultaneously injected high concentrations of aerosols at high altitudes into the troposphere (Mereuţă et al., 2022). Based on this small number of events, it is difficult to assign a separate aerosol class for these oil smoke plumes. However, valuable information regarding

size distributions, particle depolarization ratio, and to some extent, the lidar ratio can be inferred from this study (Mereuţă et al., 2022). It should be noted that these values reflect smoke plumes located very close to the fire sources and, therefore, exhibit reduced mixing ratios with other types of aerosols present in the local atmospheric background (Mereuţă et al., 2022).

Table 5. Backscatter and extinction statistics for plume values based on CALIPSO lidar measurements.

Nr. event	Date	Backscatter coefficient (plume)						(background)	
		mean 532	STDEV 532	STER 532	mean 1064	STDEV 1064	STER 1064	mean 532	mean 1064
	01.07.2016	0.006	0.003	0.0004	0.005	0.002	0.0004	0.002	0.001
1	17.07.2016	0.007	0.002	0.0004	0.007	0.004	0.0008	0.002	0.002
	21.10.2016	0.014	0.011	0.003	0.014	0.012	0.003	0.003	0.004
11	22.08.2008	0.007	0.004	0.0006	0.008	0.005	0.0007	0.001	0.0009
13	29.12.2014	0.002	0.001	0.0005	0.002	0.001	0.0007	0.0009	0.001
14	06.01.2016	0.015	0.016	0.002	0.017	0.016	0.002	-	-

Nr. event	Date	Backscatter coefficient (plume)						(background)	
		mean 532	STDEV 532	STER 532	mean 1064	STDEV 1064	STER 1064	mean 532	mean 1064
	01.07.2016	0.312	0.155	0.022	0.238	0.129	0.018	0.116	0.090
1	17.07.2016	0.314	0.122	0.021	0.320	0.212	0.037	0.131	0.089
	21.10.2016	0.733	0.621	0.179	0.662	0.567	0.163	0.175	0.180
11	22.08.2008	0.435	0.253	0.035	0.419	0.264	0.037	0.076	0.046
13	29.12.2014	0.105	0.043	0.021	0.099	0.055	0.027	0.045	0.035
14	06.01.2016	1.659	1.823	0.268	1.554	1.588	0.234	-	-

Table 6. Mean plume values for lidar-specific aerosol properties (PDR – particulate depolarization ratio; lidar ratio) and uncertainty estimates based on CALIPSO measurements.

Nr. event	Date	PDR 532 nm (plume)	PDR 532 nm (background)	Lidar ratio 532 nm (plume)	Lidar ratio 1064 nm (plume)
	01.07.2016	0.27 ± 0.30	0.25 ± 0.70	44 ± 9	44 ± 13
1	17.07.2016	0.32 ± 0.48	0.19 ± 0.43	44 ± 9	44 ± 13
	21.10.2016	0.15 ± 0.24	0.22 ± 0.47	49 ± 15	46 ± 19
11	22.08.2008	0.11 ± 0.18	0.17 ± 0.35	55 ± 22	48 ± 24
13	29.12.2014	0.12 ± 0.14	0.12 ± 0.25	37 ± 15	37 ± 15
14	06.01.2016	0.11 ± 0.43	-	109 ± 47	86 ± 10

Table 7. Mean plume values of aerosol optical properties based on CALIPSO lidar measurements.

Nr. event	Date	AOD 532 (plume)	AOD 532 (background)	AOD 1064 (plume)	AOD 1064 (background)	AE 532/1064 (plume)	AE 532/1064 (background)	Section length (5 km)	Section height (0.06 km)
	01.07.2016	0.046 ± 0.010	0.017 ± 0.005	0.035 ± 0.014	0.013 ± 0.007	0.39	0.38	100	0.150
1	17.07.2016	0.084 ± 0.019	0.035 ± 0.007	0.086 ± 0.038	0.024 ± 0.01	-0.03	0.54	35	0.274
	21.10.2016	0.088 ± 0.029	0.021 ± 0.006	0.079 ± 0.038	0.021 ± 0.01	0.15	0.03	30	0.120
11	22.08.2008	0.163 ± 0.066	0.028 ± 0.012	0.157 ± 0.08	0.017 ± 0.009	0.05	0.71	40	0.375
13	29.12.2014	0.025 ± 0.010	0.008 ± 0.003	0.023± 0.017	0.010 ± 0.06	0.12	-0.32	5	0.240
14	06.01.2016	1.526 ± 0.804	Clean air	1.430 ± 0.473	Clean air	0.09	Clean air	15	0.920

5.5 AERONET case study

Only one study was identified in the scientific literature (Mather et al., 2007) where aerosol properties from the Bouncefield fire were measured at two distinct locations. However, we identified the smoke plume from event 10, resulting from the oil tank fires in Vasylkiv, Kiev Region, Ukraine, on June 9, 2015. The smoke plume was captured in RGB images, as shown in Figure 6. Figure 7a exhibits a distinct signature for the smoke plume, as the AOD values significantly increased at all measured wavelengths (Mereuţă et al., 2022). Figure 7c provides a good indication of particle size, as the monthly averages reveal significantly decreased AE values on the day of the event (Mereuţă et al., 2022). Figure 7d displays AE values ranging from 0.45 to 0.9, corresponding to the time interval when the smoke plume was observed. Figure 7b illustrates increasing AOD values as the smoke plume moved towards the northeast of Kiev. The AERONET station in Kiev is located approximately 35 km northeast of the Vasylkiv tank depot (Mereuţă et al., 2022). From Figure 7b, it can be observed that the main mass of smoke was detected at 9:45 UTC. At that time, the measurements indicated AOD values of 0.68 at 500 nm. Unfortunately, no inversion products were available to match direct solar measurements, as the sky above Kiev was partially cloudy during that period.

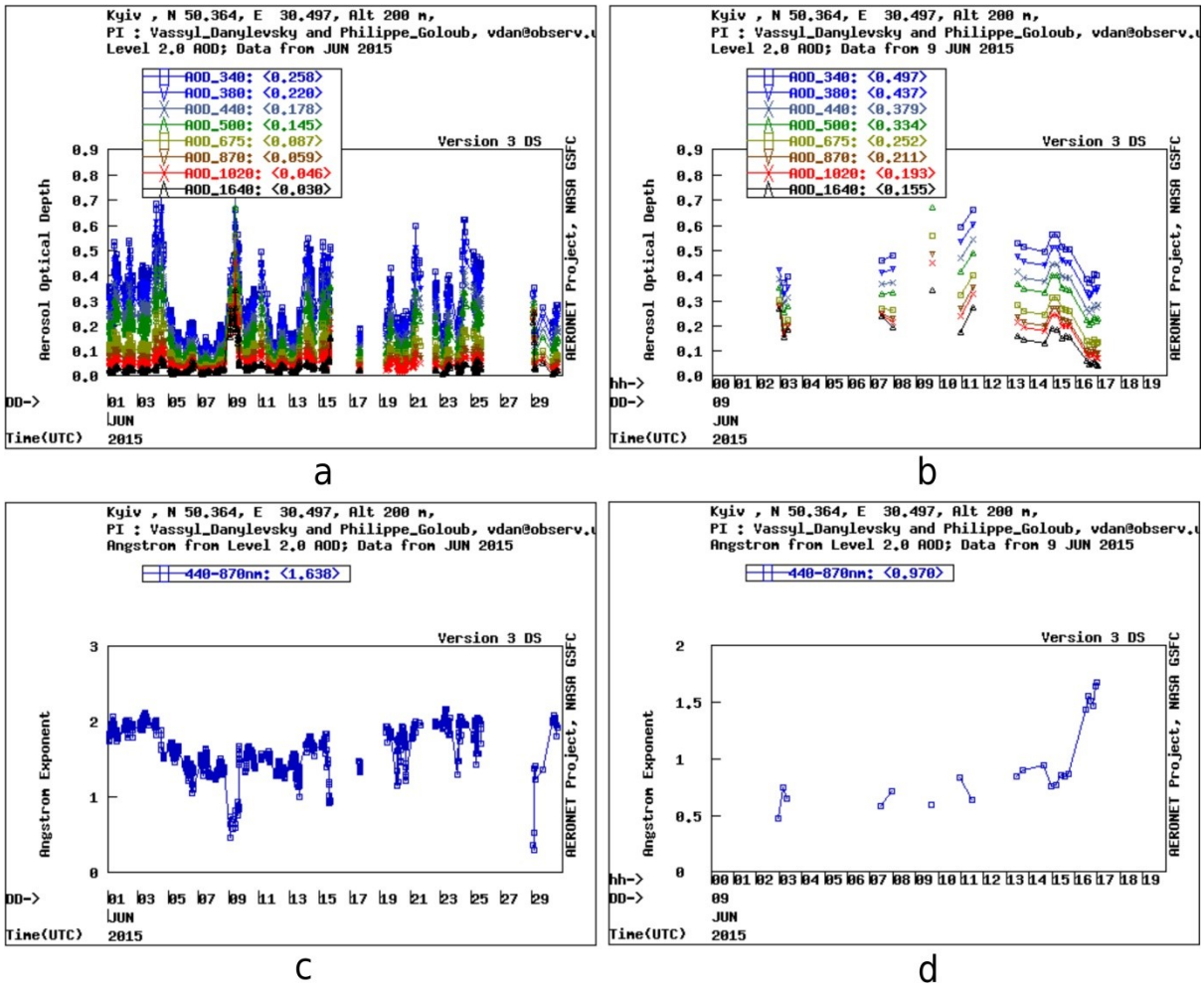

Figura 7. AOD and AE smoke plume values at Kiev on 9 June 2015 and monthly values from June 2015.

5.6 Discussions and similar studies

The results presented in this study show a wide range of values attributed to a multitude of local factors, such as background aerosols, burning rate, meteorological conditions, fuel type, retrieval timing, and local geography. Other factors can be attributed to different types of methods and algorithms used to obtain specific aerosol data (Mereuţă et al., 2022). MODIS data showed relatively low values of specific smoke plume AOD, ranging from -0.04 ± 0.04 to 0.16 ± 0.08. The only event captured by both MODIS and CALIPSO retrievals within a 2-minute time interval exhibited a high level of discrepancy (Mereuţă et al., 2022). In particular, event 14 showed average column AOD values of 0.21 ± 0.09 over

the plume region, with a maximum pixel value of 0.32 ± 0.11 (550 nm) (Mereuţă et al., 2022). In contrast, CALIPSO measurements revealed an average smoke plume AOD value of 1.52 ± 0.8 (532 nm), representing specific values as no other extinction values were detected below or above the tropospheric smoke plume in the atmospheric scene (Mereuţă et al., 2022). In the other 5 cases, CALIPSO-retrieved AOD values ranged from 0.02 ± 0.01 to 0.16 ± 0.06 for an average plume thickness ranging from 0.120 to 0.375 km (Mereuţă et al., 2022). While these values are more similar to successful MODIS retrievals, a direct comparison should be avoided. One possible reason is that MODIS did not successfully retrieve AOD values over land, thus a direct comparison with CALIPSO cannot be made for events 1 and 11 (Mereuţă et al., 2022). MODIS retrievals from event 13 on December 28 and 29, 2014 were made approximately 12 hours apart from CALIPSO retrievals. Both sensors agreed on low AOD values for the respective smoke plumes. The high levels of uncertainty in MODIS LUT values and unconstrained CALIPSO lidar solutions suggest the need for a more detailed analysis (Mereuţă et al., 2022). The only observed case with an AERONET solar photometer (event 10) indicated AOD values ranging from 0.28 to 0.68 ± 0.01 (500 nm). However, satellite imagery suggests that these values were not relevant to the main plume, which likely did not reach Kiev. However, MODIS did not successfully retrieve any AOD values for this event or any others over land, while for other events over the ocean, it did not provide such high AOD values (Mereuţă et al., 2022). We can thus deduce that MODIS AOD specific to petrochemical smoke plumes cannot yield satisfactory results, as the predefined LUT values do not encompass events similar to those described in this study.

CALIPSO AOD measurements are directly influenced by the lidar ratio. For events retrieved by CALIPSO, obtaining an accurate estimation of the lidar ratio is very challenging based on unconstrained solutions. On one hand, these lidar ratios are not directly measured (Mereuţă et al., 2022). On the other hand, the lidar ratio for smoke plumes can exhibit different behaviour, given the high content of BC (Black Carbon), which is different from biomass smoke or smoke-polluted continental aerosols. In cases of "clean" atmospheric conditions, a constrained solution may lead to a better estimation of AOD values (Mereuţă et

al., 2022). However, these conditions are rarely encountered, accounting for less than 0.01% of all detected aerosol layers (Tackett et al., 2018). When lidar ratios are directly estimated (event no. 14), uncertainties regarding opaque aerosol layers make it difficult to assess whether AOD values are overestimated or underestimated (Mereuţă et al., 2022). AE values appear to be more consistent among MODIS, CALIPSO, and AERONET, as all techniques suggest the presence of coarse aerosol mixtures. However, under conditions of low AOD values, direct comparisons with other sensors should be avoided (Mereuţă et al., 2022).

Table 8 presents the optical properties of petrochemical smoke from various studies that employed similar ground-based or airborne measurement techniques. In general, MODIS AOD estimates are very small compared to the reference studies presented in Table 8 (Mereuţă et al., 2022). It should be noted that the AOD values for smoke plumes during the Gulf War are largely higher due to the magnitude of the event. These measurements describe super-composite plumes resulting from a large number of oil well fires, blowouts, and storage tank fires (Mereuţă et al., 2022).

Table 8. Oil smoke optical properties from ground-based and flight measurements along with the scientific reference.

References	LIDAR					
	AOD 532 nm	AOD 1064 nm	AE 550/1064 nm	PDR 532 nm	LR 532 nm (sr)	LR 1064 nm (sr)
This study CALIPSO	0.025 ± 0.010 – 1.526 ± 0.804	0.023 ± 0.017 - 1.430 ± 0.473	- 0.03 – 0.39	0.11 ± 0.43 - 0.32 ± 0.48	37 ± 15 - 109 ± 47	37 ± 15 - 86 ± 10
(Okada et al. 1992) Ground based Lidar	-	-	-	0.14 – 0.18	-	-
(Ross et al. 1996) Lidar airborne	0.2 - 0.6	-	-	-	38	-
(Laursen et al. 1992) Lidar airborne	0.05 – 1 ± 65%	0.05 – 1.2 ± 85%	-	-	-	-
(Ceolato et al. 2020) Ground based Lidar	-	-	-	0.058	-	-
(Ceolato et al. 2021) Ground based Lidar	-	-	-	-	125.3±5.0 sr	-

References	Radiometer			Sun photometer		
	AOD 550 nm	**AE 550/860 nm**	**R_{eff} (µm)**	**AOD 500 nm**	**AE 440/870 nm**	**R_{eff} (µm)**
This Study MODIS & AERONET	- 0.04 – 0.16 ±(0.05 + 0.20 × AOD)	- 0.18 – 1.25	0.29 – 1.73 µm	0.28 – 0.68 ± 0.01	0.45 – 0.90	-
(Pilewskie and Valero 1992) Airborne radiometer	0.82 – 1.92 ± 2% (500 nm)	-	-	-	-	-
(Nakajima et al. 1996)	-	-	-	1.5	0.7 ± 2.5 %	-
(Mather et al. 2007)				0.3 – 1.6 (440 nm)	0.09 – 0.42	0.45 – 1.40 µm

6. PM 2.5 concentrations and și hazard map

From the previous observations, we can deduce the limitations of MODIS AOD retrieval algorithms in the case of petrochemical smoke plumes. Additionally, MODIS data is directly used by the MERRA model for reanalysis and AOD estimation in reference areas. Therefore, CALIPSO data is preferred for PM2.5 estimations.

The MERRA-2 model exhibits a high correlation between AOD and PM2.5 values observed in the background atmospheric zone, with an R^2 value of 0.9. However, the correlation decreases to $R^2 = 0.67$ for specific smoke plume values, indicating the limitations of satellite-based AOD retrieval algorithms using passive sensors. Figure 8 represents the correlated values (pixel vs pixel) of AOD and PM2.5 from MERRA-2 data for smoke plumes specific to events in the Libyan region.

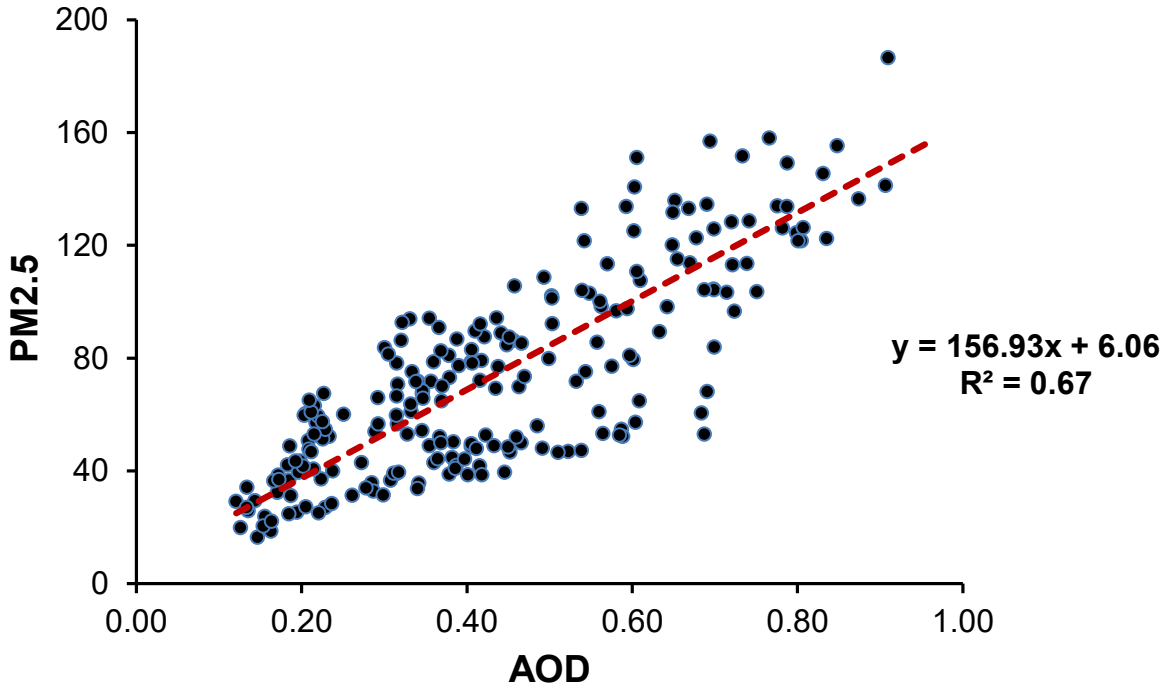

Figure 8. The correlation between PM2.5 and AOD values extracted from MERRA-2 for the events in Libya.

MERRA-2 estimates an average AOD of 0.43, which is higher than the MODIS average of 0.23 and lower than the CALIPSO average of 1.52. Based on empirical observations from this study, the AOD specific to smoke plumes exhibits values between 2 and 6 (depending on the event's characteristics and the sensor used), which are several times higher than the background atmospheric levels. Therefore, we applied a correction factor to the CALIPSO AOD values to reflect this ratio consistently in both MODIS and CALIPSO measurements. The average CALIPSO AOD becomes 1.01, and the estimated average PM2.5 concentration becomes 173 (µg/m3). The spatial distribution of these values attributed to the pixel size of MODIS AOD is presented in Figure 9.

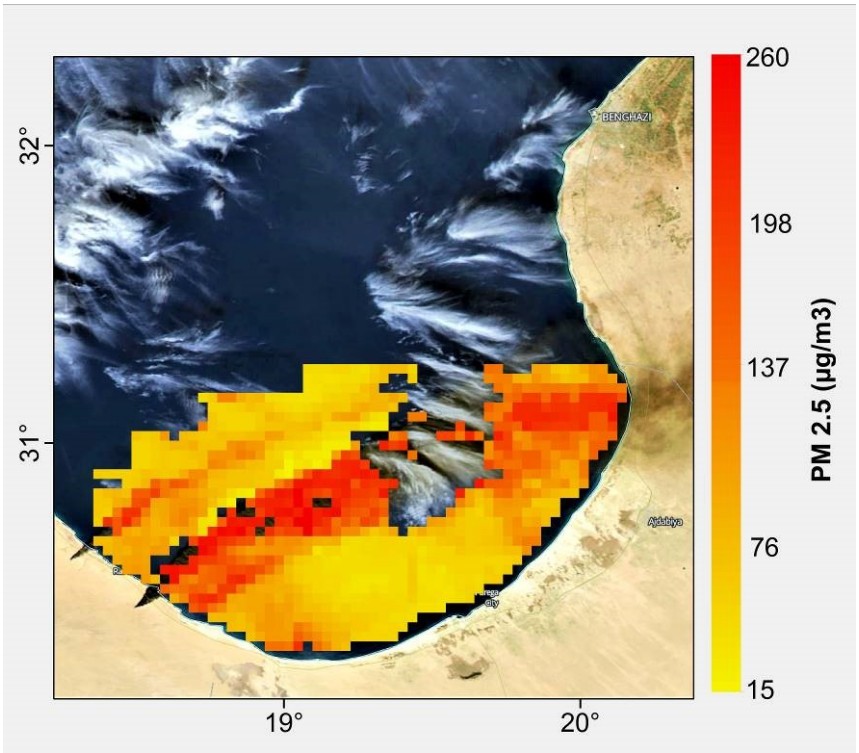

Figure 9. The estimated PM2.5 concentration for the Gulf of Sidra event on 06.10.2016.

The PM2.5 values range from 15 to 263 µg/m³, with the highest values constrained near the source and at the centre of the smoke plume. Regarding the MERRA-2 data, they were averaged over the entire observed event period, specifically from 5th to 7th January 2016. During this period, MODIS made 2 retrievals while CALIPSO made one retrieval.

Therefore, the PM2.5 values cannot be considered as daily or hourly averages; they reflect estimations over a 3-day period from the MERRA-2 reanalysis, corrected by a constrained retrieval.

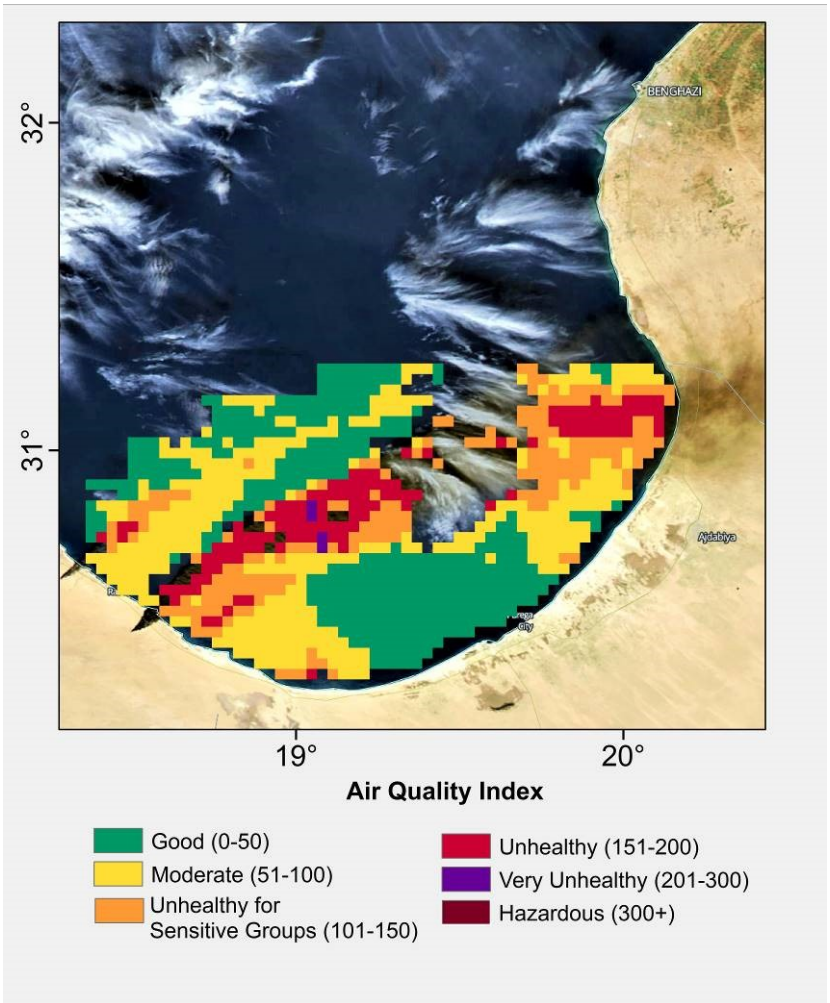

Figure 10. The Air Quality Index (AQI) calculated based on the PM2.5 estimations for the Gulf of Sidra event on October 6, 2016.

Figure 10 shows a significant area of influence where air quality deteriorates and is considered unhealthy. Considering the uncertainty in CALIPSO AOD retrieval and the applied correction factor, these intervals have a qualitative nature with a certain degree of conservatism. To obtain estimates that are closer to reality, it is necessary to reduce uncertainties in satellite retrievals and introduce specific constraints in reanalysis models. The

hazard map obtained in this study presents promising results for the use of synergistic satellite observations in assessing risks associated with petrochemical smoke plumes.

7. Conclusions

In this study, we examined smoke plumes from 30 major industrial events over a 12-year period. To our knowledge, this is the first study to employ a synergistic approach based on satellite remote sensing techniques (Mereuţă et al., 2022). The MODIS algorithm over the ocean successfully retrieved aerosol properties in 10 cases, ranging on average from -0.06 to 0.16 for plume-specific AOD, -0.18 to 1.25 for the Angstrom exponent, and 0.29 to 1.73 μm for the effective radius. Except for event 4, all smoke plumes exhibited AE values below 0.74, suggesting predominantly coarse mode smoke particles. CALIPSO measurements showed plume AOD values ranging from 0.02 to 0.16 (532 nm) and 0.02 to 0.15 (1064 nm), except for one event where AOD values reached 1.52 (532 nm) and 1.43 (1064 nm) (Mereuţă et al., 2022). AE values varied from -0.03 to 0.39, which is in agreement with MODIS. A large discrepancy was found for event 14, where CALIPSO AOD values were five times higher than MODIS. For this specific event, CALIPSO retrieved high lidar ratios of 109 ± 47 (532 nm) and 86 ± 10 sr (1064 nm) based on a constrained retrieval scheme for opaque aerosol layers (Mereuţă et al., 2022). The high water vapor concentration emitted by the oil fire could have contributed to the formation of small clouds above the smoke plume and, thus, contaminated the retrievals. Typically, lidar ratios ranged from 37 to 55 sr (532 nm) and 37 to 48 sr (1064 nm), however, these unconstrained solutions indicated scene-specific aerosol values. The particle extinction coefficient values varied between 0.10 and 1.65 km^{-1} (532 nm) and between 0.10 and 1.55 km^{-1} (1064 nm). On average, backscatter and extinction coefficients were 2 to 9 times higher than the local background (Mereuţă et al., 2022). The particle depolarization ratios varied between 0.11 and 0.15 for four out of six cases, while the other cases produced higher values of 0.27 and 0.32. We suspect that this discrepancy in the two cases at Qayyara is a result of dust aerosols present in the local background atmosphere.

The values presented are consistent with similar studies that utilized ground-based and airborne measurements (Mereuţă et al., 2022). We believe that MODIS provides a conservative estimation of plume-specific AOD because the MODIS algorithms are based on general aerosol models and various atmospheric conditions from lookup tables, which do not reflect the light-absorbing nature of these smoke plumes. Additionally, the spectral reflectance relationship used by MODIS algorithms may hinder most retrieval attempts as smoke plumes with high BC content exhibit a distinct spectral signature. CALIPSO measurements heavily rely on unconstrained lidar solutions, which in turn do not accurately reflect the reality of smoke plumes (Mereuţă et al., 2022). Therefore, we believe that AOD values based on CALIPSO measurements are of a conservative nature, as smoke with strong absorbing properties in the visible range would produce higher lidar ratios and AOD values. In general, constrained retrievals would better reflect the actual properties of the smoke, as they are not based on an ad-hoc assignment of the lidar ratio. However, assigning a constrained retrieval to petrochemical smoke plumes requires two conditions: 1) the plume should be surrounded by clean air, and 2) the smoke concentrations should not exceed a threshold where total attenuation occurs (Mereuţă et al., 2022). Additionally, the magnitude of the event is an important factor as the smoke plumes need to reach the necessary temperature to penetrate the PBL. The lidar ratios generated from event 14 represent an extremely rare occurrence where the smoke plumes were treated as a layer of opaque aerosols. Therefore, it was challenging to assess whether the lidar ratios are overestimated or underestimated, although we believe that this current solution is still preferable to unconstrained solutions (Mereuţă et al., 2022). We emphasize the need for additional lidar measurements of smoke plumes, as based on this study, we cannot conclude whether these aerosols belong to a distinct subtype of smoke. Future spaceborne lidar missions, such as EarthCare (Illingworth et al., 2015), will provide direct measurements of lidar ratios and the opportunity for better AOD estimates regarding these types of events (Mereuţă et al., 2022). Based on this study, we have concluded that the ground-based MODIS algorithms are not yet suitable for retrieving the properties of petrochemical smoke aerosols due to their strong

light-absorbing properties. This study has demonstrated a novel method for identifying and analysing smoke plumes, which, in some cases, do not require potentially hazardous field campaigns. We believe that these types of studies strongly indicate the need for improving models and algorithms for acquiring atmospheric aerosols. For these types of aerosols, better AOD estimates are important both for air quality and implications for climate change (Mereuţă et al., 2022).

Utilizing reanalysis model data, such as MERRA-2 or CAMS, can provide an additional advantage in estimating emissions of specific pollutants from petrochemical smoke. Within this thesis, MERRA-2 data were analysed and proved to be more capable of distinguishing a relative increase in PM2.5 emissions and AOD following petrochemical smoke release events. Unlike MODIS data, MERRA-2 estimated higher AOD values, although they were considerably lower than the AOD estimated by CALIPSO for event 14. For this reason, a hybrid method combining MERRA-2 data and CALIPSO-corrected data was used to estimate PM2.5 concentrations. As a result, event 14 recorded PM2.5 values ranging from 15 to 263 μg/m3. The hazard map delineated based on these estimations reveals a significant area exposed to unhealthy air quality conditions. Taking into account CALIPSO data, it can be concluded that the elevation of the smoke plume (ranging from 2-4 km) acted as a mitigating factor for the risk of high concentrations of particulate matter exposure. This study highlights the necessity of synergizing atmospheric data for a more holistic analysis and quantification of both the properties and concentrations of pollutants of interest and their proximity to potential risk-exposed elements.

The satellite observations presented in this thesis provide a suite of unique measurable characteristics that can be successfully used to validate models estimating the effects and consequences of petrochemical smoke. Thus, through more robust models, we can associate a more realistic level of risk in the case of exposure to petrochemical smoke. Additionally, accurate quantification of this type of aerosol can lead to improvements in satellite retrieval methods. Regarding air quality studies, this research can introduce a new technique for observing black carbon and can be synergistically used to describe the temporal and spatial

evolution of such pollutant plumes. Advances in satellite sensor technology can provide added value in the form of near-real-time data, aiding in the efficiency of disaster response efforts. In this regard, the doctoral thesis can represent an important milestone in developing a calibrated retrieval algorithm for developing an early warning system associated with atmospheric aerosols.

Within the scope of this doctoral thesis, a database has been developed that encompasses significant major industrial accidents in the global petrochemical industry from 2008 to 2020. These events are individually detailed and identified based on location, typology, and causality. This information, along with the spatiotemporal evolution of smoke plumes, is of great interest for studies in the field of industrial risk analysis and NaTech (Natural-Technological) hazards. In the case of predictive modelling techniques, historical accident data play an important role in both model validation and optimization.

References

Andreae, M.O., 2019. Emission of trace gases and aerosols from biomass burning – an updated assessment. Atmospheric Chem. Phys. 19, 8523–8546. https://doi.org/10.5194/acp-19-8523-2019

Brauer, M., Freedman, G., Frostad, J., Van Donkelaar, A., Martin, R.V., Dentener, F., Dingenen, R.V., Estep, K., Amini, H., Apte, J.S., Balakrishnan, K., Barregard, L., Broday, D., Feigin, V., Ghosh, S., Hopke, P.K., Knibbs, L.D., Kokubo, Y., Liu, Y., Ma, S., Morawska, L., Sangrador, J.L.T., Shaddick, G., Anderson, H.R., Vos, T., Forouzanfar, M.H., Burnett, R.T., Cohen, A., 2016. Ambient Air Pollution Exposure Estimation for the Global Burden of Disease 2013. Environ. Sci. Technol. 50, 79–88. https://doi.org/10.1021/acs.est.5b03709

Ceolato, R., Bedoya-Velásquez, A.E., Fossard, F., Mouysset, V., Paulien, L., Lefebvre, S., Mazzoleni, C., Sorensen, C., Berg, M.J., Yon, J., 2022. Black carbon aerosol number and mass concentration measurements by picosecond short-range elastic backscatter lidar. Sci. Rep. 12, 8443. https://doi.org/10.1038/s41598-022-11954-7

Ceolato, R., Paulien, L., Maughan, J.B., Sorensen, C.M., Berg, M.J., 2020. Radiative properties of soot fractal superaggregates including backscattering and depolarization. J. Quant. Spectrosc. Radiat. Transf. 247, 106940. https://doi.org/10.1016/j.jqsrt.2020.106940

Daum, P.H., Al-Sunaid, A., Busness, K.M., Hales, J.M., Mazurek, M., 1993. Studies of the Kuwait oil fire plume during midsummer 1991. J. Geophys. Res. 98, 16809. https://doi.org/10.1029/93JD01204

Dutkiewicz, V.A., Alvi, S., Ghauri, B.M., Choudhary, M.I., Husain, L., 2009. Black carbon aerosols in urban air in South Asia. Atmos. Environ. 43, 1737–1744. https://doi.org/10.1016/j.atmosenv.2008.12.043

Ferek, R.J., Hobbs, P.V., Herring, J.A., Laursen, K.K., Weiss, R.E., Rasmussen, R.A., 1992. Chemical composition of emissions from the Kuwait oil fires. J. Geophys. Res. 97, 14483. https://doi.org/10.1029/92JD01247

Finer, M., Novoa, S., Weisse, M.J., Petersen, R., Mascaro, J., Souto, T., Stearns, F., Martinez, R.G., 2018. Combating deforestation: From satellite to intervention. Science 360, 1303–1305. https://doi.org/10.1126/science.aat1203

Gullett, B.K., Aurell, J., Holder, A., Mitchell, W., Greenwell, D., Hays, M., Conmy, R., Tabor, D., Preston, W., George, I., Abrahamson, J.P., Vander Wal, R., Holder, E., 2017. Characterization of emissions and residues from simulations of the Deepwater Horizon surface oil burns. Mar. Pollut. Bull. 117, 392–405. https://doi.org/10.1016/j.marpolbul.2017.01.083

Gullett, B.K., Hays, M.D., Tabor, D., Wal, R.V., 2016. Characterization of the particulate emissions from the BP Deepwater Horizon surface oil burns. Mar. Pollut. Bull. 107, 216–223. https://doi.org/10.1016/j.marpolbul.2016.03.069

Gupta, P., Remer, L.A., Levy, R.C., Mattoo, S., 2018. Validation of MODIS 3 km land aerosol optical depth from NASA's EOS Terra and Aqua missions. Atmospheric Meas. Tech. 11, 3145–3159. https://doi.org/10.5194/amt-11-3145-2018

Haarig, M., Ansmann, A., Baars, H., Jimenez, C., Veselovskii, I., Engelmann, R., Althausen, D., 2018. Depolarization and lidar ratios at 355, 532, and 1064 nm and microphysical properties of aged tropospheric and stratospheric Canadian wildfire smoke. Atmospheric Chem. Phys. 18, 11847–11861. https://doi.org/10.5194/acp-18-11847-2018

Hobbs, P.V., Radke, L.F., 1992. Airborne Studies of the Smoke from the Kuwait Oil Fires. Science 256, 987–991. https://doi.org/10.1126/science.256.5059.987

Holben, B.N., Eck, T.F., Slutsker, I., Tanré, D., Buis, J.P., Setzer, A., Vermote, E., Reagan, J.A., Kaufman, Y.J., Nakajima, T., Lavenu, F., Jankowiak, I., Smirnov, A., 1998. AERONET—A Federated Instrument Network and Data Archive for Aerosol Characterization. Remote Sens. Environ. 66, 1–16. https://doi.org/10.1016/S0034-4257(98)00031-5

Illingworth, A.J., Barker, H.W., Beljaars, A., Ceccaldi, M., Chepfer, H., Clerbaux, N., Cole, J., Delanoë, J., Domenech, C., Donovan, D.P., Fukuda, S., Hirakata, M., Hogan, R.J., Huenerbein, A., Kollias, P., Kubota, T., Nakajima, T., Nakajima, T.Y., Nishizawa, T., Ohno, Y., Okamoto, H., Oki, R., Sato, K., Satoh, M., Shephard, M.W., Velázquez-Blázquez, A., Wandinger, U., Wehr, T., Van Zadelhoff, G.-J., 2015. The EarthCARE Satellite: The Next Step Forward in Global Measurements of Clouds, Aerosols, Precipitation, and Radiation. Bull. Am. Meteorol. Soc. 96, 1311–1332. https://doi.org/10.1175/BAMS-D-12-00227.1

Kim, M.-H., Omar, A.H., Tackett, J.L., Vaughan, M.A., Winker, D.M., Trepte, C.R., Hu, Y., Liu, Z., Poole, L.R., Pitts, M.C., Kar, J., Magill, B.E., 2018. The CALIPSO version 4 automated aerosol classification and lidar ratio selection algorithm. Atmospheric Meas. Tech. 11, 6107–6135. https://doi.org/10.5194/amt-11-6107-2018

Konovalov, I.B., Lvova, D.A., Beekmann, M., Jethva, H., Mikhailov, E.F., Paris, J.-D., Belan, B.D., Kozlov, V.S., Ciais, P., Andreae, M.O., 2018. Estimation of black carbon emissions from Siberian fires using satellite observations of absorption and extinction optical depths. Atmospheric Chem. Phys. 18, 14889–14924. https://doi.org/10.5194/acp-18-14889-2018

Laumbach, R.J., Kipen, H.M., 2012. Respiratory health effects of air pollution: Update on biomass smoke and traffic pollution. J. Allergy Clin. Immunol. 129, 3–11. https://doi.org/10.1016/j.jaci.2011.11.021

Li, S., Kahn, R., Chin, M., Garay, M.J., Liu, Y., 2015. Improving satellite-retrieved aerosol microphysical properties using GOCART data. Atmospheric Meas. Tech. 8, 1157–1171. https://doi.org/10.5194/amt-8-1157-2015

Mather, T.A., Harrison, R.G., Tsanev, V.I., Pyle, D.M., Karumudi, M.L., Bennett, A.J., Sawyer, G.M., Highwood, E.J., 2007. Observations of the plume generated by the December 2005 oil depot explosions and prolonged fire at Buncefield (Hertfordshire, UK) and associated atmospheric changes. Proc. R. Soc. Math. Phys. Eng. Sci. 463, 1153–1177. https://doi.org/10.1098/rspa.2006.1810

Mereuţă, A., Ajtai, N., Radovici, A.T., Papagiannopoulos, N., Deaconu, L.T., Botezan, C.S., Ştefănie, H.I., Nicolae, D., Ozunu, A., 2022. A novel method of identifying and analysing oil smoke plumes based on MODIS and CALIPSO satellite data. Atmospheric Chem. Phys. 22, 5071–5098. https://doi.org/10.5194/acp-22-5071-2022

Muthike, D., 2015. Satellite Earth Observations in Support of Disaster Risk Reduction Special 2015 WCDRR Edition. https://doi.org/10.13140/RG.2.1.3032.9046

Nakajima, T., Hayasaka, T., Higurashi, A., Hashida, G., Moharram-Nejad, N., Najafi, Y., Valavi, H., 1996. Aerosol Optical Properties in the Iranian Region Obtained by Ground-Based Solar Radiation Measurements in the Summer Of 1991. J. Appl. Meteorol. Climatol. 35, 1265–1278. https://doi.org/10.1175/1520-0450(1996)035<1265:AOPITI>2.0.CO;2

Okada, K., Ikegami, M., Uchino, O., Nikaidou, Y., Zaizen, Y., Tsutsumi, Y., Makino, Y., 1992. Extremely high proportions of soot particles in the upper troposphere over Japan. Geophys. Res. Lett. 19, 921–924. https://doi.org/10.1029/92GL00487

Pilewskie, P., Valero, F.P.J., 1992. Radiative effects of the smoke clouds from the Kuwait oil fires. J. Geophys. Res. 97, 14541. https://doi.org/10.1029/92JD01371

Ramanathan, V., Carmichael, G., 2008. Global and regional climate changes due to black carbon. Nat. Geosci. 1, 221–227. https://doi.org/10.1038/ngeo156

Ross, J.L., Waggoner, A.P., Hobbs, P.V., Ferek, R.J., 1996. Airborne Lidar Measurements of a Smoke Plume Produced by a Controlled Burn of Crude Oil on the Ocean. J. Air Waste Manag. Assoc. 1995 46, 327–334. https://doi.org/10.1080/10473289.1996.10467467

Samset, B.H., Stjern, C.W., Andrews, E., Kahn, R.A., Myhre, G., Schulz, M., Schuster, G.L., 2018. Aerosol Absorption: Progress Towards Global and Regional Constraints. Curr. Clim. Change Rep. 4, 65–83. https://doi.org/10.1007/s40641-018-0091-4

Sogacheva, L., Popp, T., Sayer, A.M., Dubovik, O., Garay, M.J., Heckel, A., Hsu, N.C., Jethva, H., Kahn, R.A., Kolmonen, P., Kosmale, M., De Leeuw, G., Levy, R.C., Litvinov, P., Lyapustin, A., North, P., Torres, O., Arola, A., 2020. Merging regional and global aerosol optical depth records from major available satellite products. Atmospheric Chem. Phys. 20, 2031–2056. https://doi.org/10.5194/acp-20-2031-2020

Stevens, R., Pinto, J., Mamane, Y., Ondov, J., Abdulraheem, M., Al-Majed, N., Sadek, M., Cofer, W., Ellenson, W., Kellogg, R., 1993. Chemical and Physical Properties of Emissions from Kuwaiti Oil Fires. Water Sci. Technol. 27, 223–233. https://doi.org/10.2166/wst.1993.0555

Tackett, J.L., Winker, D.M., Getzewich, B.J., Vaughan, M.A., Young, S.A., Kar, J., 2018. CALIPSO lidar level 3 aerosol profile product: version 3 algorithm design. Atmospheric Meas. Tech. 11, 4129–4152. https://doi.org/10.5194/amt-11-4129-2018

Tassa, A., 2020. The socio-economic value of satellite earth observations: huge, yet to be measured. J. Econ. Policy Reform 23, 34–48. https://doi.org/10.1080/17487870.2019.1601565

Wei, X., Chang, N.-B., Bai, K., Gao, W., 2020. Satellite remote sensing of aerosol optical depth: advances, challenges, and perspectives. Crit. Rev. Environ. Sci. Technol. 50, 1640–1725. https://doi.org/10.1080/10643389.2019.1665944

Young, S.A., Vaughan, M.A., Garnier, A., Tackett, J.L., Lambeth, J.D., Powell, K.A., 2018. Extinction and optical depth retrievals for CALIPSO's Version 4 data release. Atmospheric Meas. Tech. 11, 5701–5727. https://doi.org/10.5194/amt-11-5701-2018

Zhang, K., Batterman, S., 2013. Air pollution and health risks due to vehicle traffic. Sci. Total Environ. 450–451, 307–316. https://doi.org/10.1016/j.scitotenv.2013.01.074